https://doi.org/10.5194/wes-2026-21
Preprint. Discussion started: 12 February 2026

Open Access
WIND ENERGY SCIENCE
DISCUSSIONS

Characterizing Coastal Turbulence and Wind Speed Gradients Using an Anemometer Array to Improve Offshore Wind Energy Assessment

Henry Potter[1,2] and Beibei E[1].

[1]Texas A&M University Department of Oceanography

[2]Texas A&M Geochemical and Environmental Research Group

Correspondence to: Henry Potter (hpotter@tamu.edu)

Abstract. As interest and investment in offshore wind farms increase, it becomes essential to better understand how interactions at the air-sea interface impact wind and turbulence in the marine boundary layer. Central to this effort is understanding the role of waves, especially on the relatively shallow continental shelves where most wind farms are located and waves are shaped by bathymetry. To address this, we analysed hundreds of hours of high frequency wind speeds measured by an anemometer array on a coastal tower from 14 to 26 m above the mean water surface. Wind speed gradients diverge substantially from established values, and the boundary layer was found non-constant ~60% of the time. This means that the assumptions required for applying Monin Obukhov Similarity Theory cannot be met, so wind speeds aloft cannot be accurately predicted using this canonical methodology. Wind speed gradients were highest during alongshore winds and lowest during onshore. This occurred because waves refract and shoal parallel to shore which increases surface roughness independent of wind. Onshore winds cross the waves and create strong wind–wave coupling, while alongshore winds move along the waves, weakening the coupling and reducing effective roughness. Changes in the roughness then alters the wind speed which propagated through the boundary layer impacting winds aloft. The results of this study should be used to inform wind farm siting to optimize energy yield.

Short Summary. We studied coastal winds and found that waves strongly altered wind patterns. Wind speeds increased with height faster during alongshore winds and more slowly during onshore winds. This occurred because the interaction between wind and waves was impacted by their relative directions. Consequently, common wind speed prediction methods failed much of the time. These findings showed that waves must be considered to better plan wind farm locations and improve energy production.

1 Introduction

Fluxes of momentum, which transfer energy from the wind across the air-sea interface, have been extensively studied and

https://doi.org/10.5194/wes-2026-21
Preprint. Discussion started: 12 February 2026

parameterized over the open ocean (e.g., Smith et al., 1992, Edson et al. 2013, Potter, 2015). Near the coast, fluxes differ markedly from those further offshore due to the ocean's response to bathymetric changes and the abrupt transition to land that disrupts the horizontal homogeneity typically assumed over deep water (e.g., Shabani et al., 2014; Ortiz-Suslow et al., 2015; Lentz et al., 2017; Grachev et al., 2018; Potter et al., 2022; Chen et al., 2024). Despite this, little research has focused on how these coastal conditions influence flux and wind speed profiles. Moreover, because the assumption of horizontal homogeneity, which is central to Monin-Obukhov Similarity Theory (MOST, Monin & Obukhov, 1954), cannot be met, the flux layer may deviate with height leading to departures from the canonical log-linear wind profile. This poses a challenge for two key reasons. Firstly, it undermines our ability to compare measurements taken at different heights or locations, which rely on similarity theory to convert to the standard 10 m neutral equivalent wind speed. Secondly, it limits our understanding of the true potential for wind energy capture in coastal environments because it makes it difficult to predict turbulence and wind speed aloft which are key to wind resource assessment, turbine siting, and optimizing energy yield. This paper is an investigation into the unique characteristics of coastal winds with a focus on how air-sea interactions affect profiles of wind speed and turbulence.

1.2 Background

1.2.1 Fluxes and Similarity Theory

The momentum flux $\vec{\tau}$ is the vertical transport of horizontal momentum. It can be determined from high frequency measurements of wind velocity in the horizontal-downwind, -crosswind, and vertical directions, u, v, and w, respectively,

$$\vec{\tau} = \rho\left[\left(-\overline{u'w'}\right)\vec{\imath} + \left(-\overline{v'w'}\right)\vec{\jmath}\right]. \tag{1}$$

Here, ρ is the air density, $\vec{\imath}$ and $\vec{\jmath}$ are unit vectors along and perpendicular to the mean wind direction, overbar represents a time average, and primes denote fluctuating components. The flux can also be represented in terms of the friction velocity which was introduced by Monin and Obukhov (1954) as a turbulent scaling parameter,

$$u_* = \frac{\sqrt{|\tau|}}{\rho}. \tag{2}$$

Monin–Obukhov Similarity Theory suggests that in the lower boundary layer where the flux is constant, and when conditions are stationary and horizontally homogenous (i.e., flat homogenous terrain, uniform roughness, and fair weather), the vertical gradient of wind speed is related to the friction velocity through a universal dimensionless gradient function Φ_u,

$$\Phi_u(\zeta) = \frac{\kappa z}{u_*}\left(\frac{\partial U}{\partial z}\right). \tag{3}$$

U is the mean wind speed, z is measurement height, κ is the Von Kármán constant ≈ 0.41, and $\zeta = z/L$, where L is the Obukhov Length (Monin and Obukhov, 1954). The presence of κ in these equations is such that Φ_u (0) = 1 so that when the boundary

https://doi.org/10.5194/wes-2026-21
Preprint. Discussion started: 12 February 2026

layer is neutral the gradient function becomes obsolete. L accounts for the effects of buoyancy on the wind profile and is given by

$$L = -\frac{u_*^3\overline{\theta_v}}{\kappa g(\overline{w'\theta_v'})}\,. \tag{4}$$

Here g = 9.8 m s^{-2} is acceleration due to gravity, $\overline{\theta_v}$ is the mean virtual temperature, and $\overline{w'\theta_v'}$ is the virtual temperature flux. L represents the ratio between shear and buoyancy production of turbulence. In magnitude, L is the height at which shear-driven and buoyancy-driven turbulence are equal. L is positive for stable conditions, and negative for unstable. In neutral conditions where buoyant forcing becomes negligible, $|z/L|$ goes to 0 whereby Φu in Eq. (3) becomes zero, yielding the classic logarithmic mean wind profile,

$$\frac{\partial U}{\partial z} = \frac{u_*}{\kappa z}. \tag{5}$$

Monin and Obukhov (1954) suggested that the gradient function should be determined experimentally. Integrating Eq. (3), the velocity profile becomes,

$$U_z - U_0 = \frac{u_*}{\kappa}\left[\ln\left(\frac{z}{z_0}\right) - \psi_u(\zeta)\right]. \tag{6}$$

U_0 is the mean wind speed at the surface, z_0 is the roughness length for momentum and $\psi_u(\zeta)$ is the integrated form of $\varphi_u(\zeta)$. Employing Eqs. (4&5), wind speeds can be converted to 10 m neutral-equivalent U_{10N}.

A cluster of experiment in Australia were some of the first to calculate the MOST gradient functions (Swinbank, 1964; Swinbank and Dyer, 1966; Webb, 1970; Dryer and Hicks, 1970). The sites were all terrestrial with acres of low vegetation including 2-inch barley grass, a ploughed wheat farm, and dead grass of uniform 6-10 cm over flat sheep grazing country. Around the same time the Kansas Field Program (Izumi, 1968) took place. This was at a square-mile of flat farmland covered with 18-cm wheat stubble and led to the oft-adopted gradient functions originated by Bursinger et al. (1971). These were revised by Högström (1988) and later by Kitaigorodskii and Donelan (1984) using a theoretical approach. In all the experimental cases it is easy to see that the MOST conditions—flat, uniform terrain and constant flux—are met. At sea where the surface is dynamic, meeting these requirements is less certain. Alluding to this, Drennan (2006) wrote *"The air-sea interface is fundamentally different from the air-land interface in that the roughness elements are mobile, and evolve with both the atmosphere and ocean."* Nonetheless, for sake of simplicity or necessity, oceanographers and marine meteorologists readily adopt MOST. The widely applied Coupled Ocean-Atmosphere Response Experiment (COARE) algorithm (Edson et al. 2013) uses the gradient functions from Beljaars and Holtslag (1991) which were developed over land. Using profiles of wind and fluxes during three experiments Edson et al. (2013) found MOST is mostly valid over the open ocean. This result was restricted to wave age (C_p/U, where C_p is peak frequency wave speed) < 2.5 because under light winds, fast swell can modify the wind profile (e.g., Sullivan et al. 2008). In contrast, Ortiz-Suslow et al. (2021) used an anemometer array on the

https://doi.org/10.5194/wes-2026-21
Preprint. Discussion started: 12 February 2026

Floating Instrument Platform (FLIP) to show that only 30-40% of momentum flux gradients were constant at sea. Vertical flux variability was most common during wind-swell alignment. Moreover, Lyu et al. (2024) showed that gustiness is also associated with the breakdown of the constant flux layer over the ocean.

At the coast, waves shoal and break as the ocean transitions to land. This heterogeneity means the nearshore cannot adhere to the spatial uniformity required by MOST (Grachev et al., 2018). The flux is sourced over an upwind region called the flux footprint. Flux footprints are positively skewed normal distributions with a peak and approximate upper and lower bounds over some range (*O* 10s-100s m). When fluxes are recorded close to the ground, the footprint is typically small with a nearby peak. As measurement height increases the flux peak and footprint become increasingly distant. Hence, instrument height alters the range of surface conditions influencing the measured flux, each uniquely impacting momentum exchange. The consequence is that when two or more flux measurements are made simultaneously along the coast, each records fluxes sourced over different surface conditions, so the flux will change with height, i.e., will not be constant.

Though the nearshore is studied little with the explicit intent of examining or validating MOST, results have shown that an internal boundary layer (IBL) is formed for both onshore and offshore flow. For onshore wind the IBL develops when air flows over the ocean and onto land and begins to adjust to the new, rougher surface. The IBL forms near the ground as flow adjusts to the terrestrial surface and grows vertically as the air moves inland. This can impact the momentum exchange due to different surface types which decouple the boundary layer. Shabani et al. (2014), Grachev at al. (2018) and Potter et al (2025) have all identified a coastal IBL for onshore wind at heights that depend upon the wind angle and beach characteristics. Grachev et al. (2018) suggested that MOST is inappropriate along the coast because of non-local transport which causes the decoupling aloft. For offshore flow of warm air over cooler water, the turbulence in the IBL is suppressed due to stable stratification which reduces sea surface roughness (e.g., Fairall et al., 2006). This decreases momentum flux compared to that predicted by MOST (Mahrt et al., 1998) because the upper boundary layer decouples from the surface (e.g., Smedman et al., 1997) potentially leading to a low-level wind speed maximum (Smedman et al., 1995). The momentum flux is also sensitive to land topography, even with onshore wind (Yang et al., 2018).

Evidently, MOST is flawed near the shore because the assumption of a constant flux layer is violated. This is a problem because comparing data from different studies requires unification, which is normally afforded by scaling winds to 10-m neutral equivalent conditions (Eq. 6). This limits our ability to predict the true impact of wind forcing on the ocean or any wind-driven process near the shore. Highly resolved $\delta U/\delta z$ is needed to improve correspondence of Φu with MOST to identify deviations from expected scaling behaviour and refine wind speed estimates and turbulence parameterizations in coastal environments.

https://doi.org/10.5194/wes-2026-21
Preprint. Discussion started: 12 February 2026

eawe european academy of wind energy
Open Access WIND ENERGY SCIENCE DISCUSSIONS

3 Experiment and Data

3.1 The Experiment

Data was collected in collaboration with the U.S. Army Research and Development Center's Field Research Facility (FRF), Duck, NC during DUNEX (DUring Nearshore Event eXperiment). FRF comprehensively monitors the coastal ocean including waves, tides, currents, sediments, bathymetry, and standard oceanic and atmospheric information. Much of this data was collected from a pier that extends 500 m offshore to the ~6 m depth contour. The wave data we used in this research were recorded by FRF using an array of pressure sensors mounted adjacent to the pier at the 4 m isobath. The instrument is hard-wired to shore, and data are analysed hourly. The seaward face at FRF is 72° from north and the shelf is wide with a gentle slope of approximately 1/1000 (Long and Oltman-Shay, 1991). Typical wave periods at FRF are 8-10 seconds with waves beginning to be influenced by the bottom at depths 50-75 m and become shallow water waves at 5-8 m, around 500 m from the shoreline. Approximately 40 m inland from the shoreline is a beach tower principally used for optical remote sensing to make nearshore measurements (Holman and Stanley, 2007). Upon this tower we mounted four new Gill R3-50 sonic anemometers 14.4, 18.4, 22.4, and 26.4 m above mean water level. These were deployed from October 2021 to January 2023. All anemometers had intermittent gaps of days to weeks in their record, so the data aren't continuous over this period. Each anemometer was powered by a solar panel and hard-wired to one of two CR1000X Datalogger also connected to solar panels. Each CR1000X stored the data in 60-minute blocks to a digital memory card which was switched out approximately once a month. The anemometers recorded u, v, and w, and air temperature at 20 Hz. Data were then broken into 30-minute bins. Spikes in u, v, and w greater than three standard deviations for the mean were interpolated through, accounting for less than 0.3% of the data. The wind vectors were rotated so that u points into the mean wind direction and $\bar{v} = \bar{w} = 0$ following Golzio et al. (2019). Data were quality controlled following the standard of French et al. (2007) and Potter et al. (2015). Following Potter et al. (2022), for each run we required the coefficient of determination for the cumulative summation of the flux to be above 0.9 to ensure conditions were stationary, and we examined the Ogives, (the integral of the cospectrum) to ensure the averaging period captured all turbulent scales present. Fig. 1 shows the location of the experiment and a photo of the beach tower with the mounted anemometers.

https://doi.org/10.5194/wes-2026-21
Preprint. Discussion started: 12 February 2026

WIND ENERGY SCIENCE DISCUSSIONS

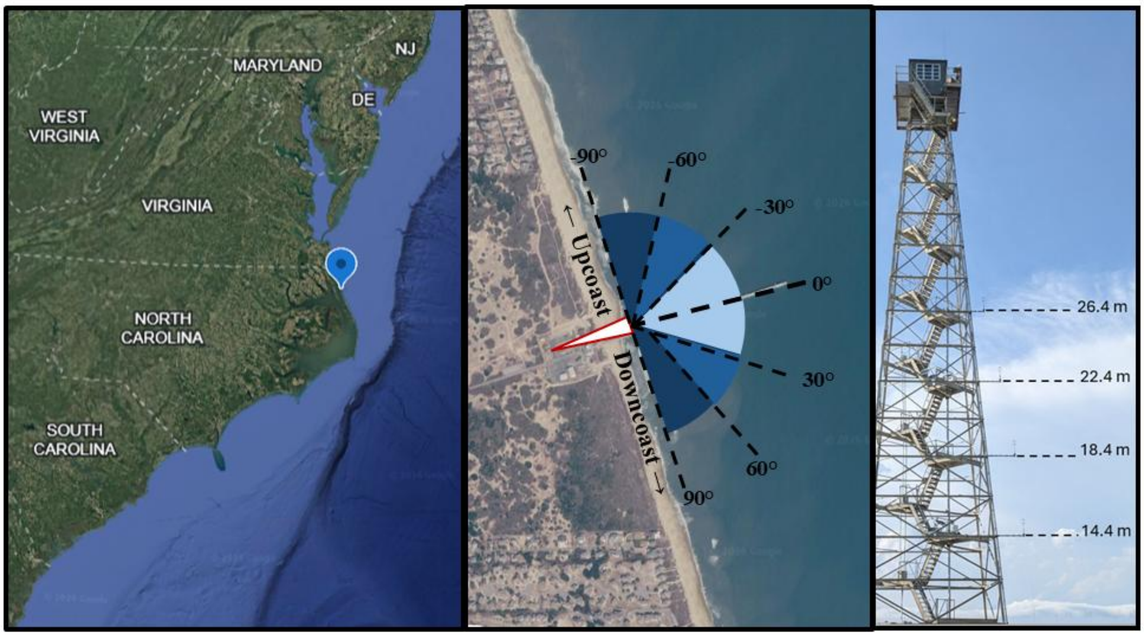

Figure 1. The location of the experiment in Duck, North Carolina is indicated by the blue pin in the left image. A close-up of the location is in the middle image which also shows how the data are segregated for analysis based on their wind direction: onshore (±30°), oblique (±30-60°), and alongshore (±60-90°). The anemometers mounted on the beach tower at the Field Research Facility from 14.4 to 26.4 m are shown in the right photo. Location of the measurement tower shown using Google Earth (version 10.96.0.1). Map data © Google.

3.2 The Data

We restricted our data to include only runs when the mean wind was ±90° from directly onshore (i.e., 72±90°). For each of these runs we calculated the flux footprint, which is detailed in Sect. 3.3. Using the upwind distance to the flux footprint maximum, and the wind direction we were able to determine if flux peak was over the beach or the ocean. Any runs with a flux peak over the beach were removed, which was most prevalent for alongshore winds. This ensured that the fluxes are oceanic and avoids internal boundary layers that can form when the surface transitions from ocean to land (e.g., Potter et al., 2025; Grachev et al., 2018). Finally, we only use the data when all four anemometers passed the data quality and wind direction standards together. This ensured that all data used in our analysis were recorded simultaneously and resulted in 1448 runs or 724 hours of data. For analysis, we rotated the frame of refence to make it shore-relative in a coming-from sense. Wind directly onshore approaches from 0°, negative values are winds approaching from upcoast, and positive values are for wind approaching from downcoast, as shown in Fig. 1. Finally, we categorized the data based on their wind direction. Runs with

https://doi.org/10.5194/wes-2026-21
Preprint. Discussion started: 12 February 2026

mean wind direction ±30° are categorized as onshore (n = 353), runs with mean wind direction ±30-60° are oblique (n = 781), and runs with mean wind direction ±60-90° are alongshore (n = 314). Figure 2 is a histogram of data distribution by direction, and the wind speed distribution is shown in Fig. 3. Most wind speeds were 4-8 m s^{-1}. Alongshore and oblique winds were recorded above 16 m s^{-1}, but maximum onshore wind was ~11 m s^{-1}.

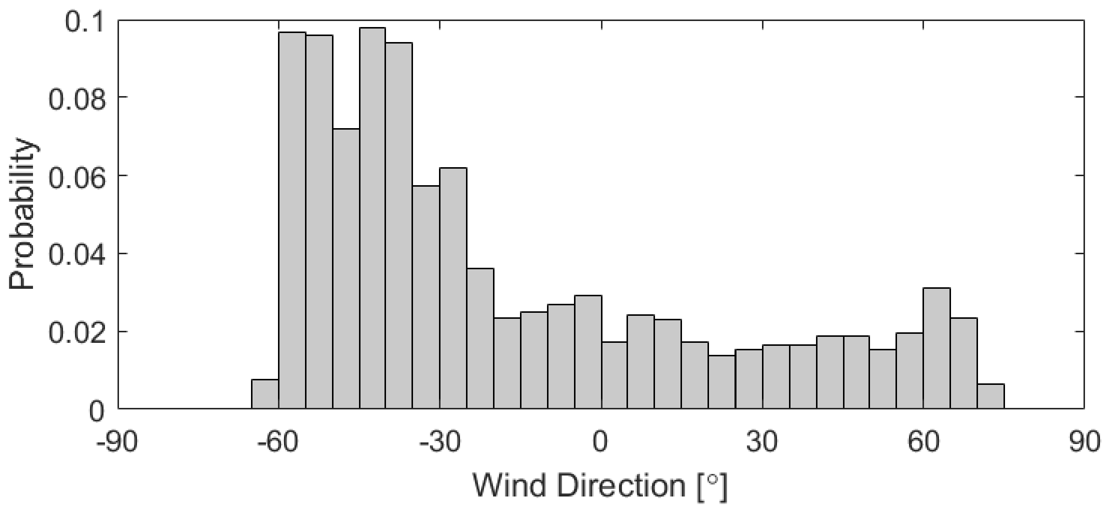

Figure 2. Histogram of wind direction normalized by probability. Of the 1448 runs, 353 are onshore (±30°), 781 are oblique (±30-60°), and 314 are alongshore (±60-90°).

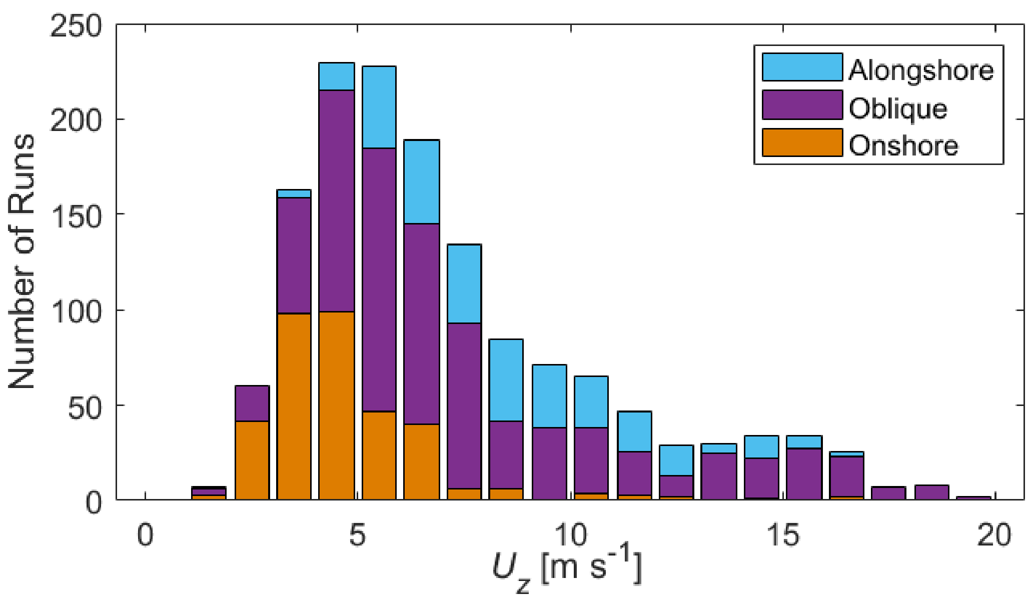

https://doi.org/10.5194/wes-2026-21
Preprint. Discussion started: 12 February 2026

Figure 3. Stacked histogram of wind speed coloured by direction.

3.3 The Flux Footprint

The flux footprint is the upwind region contributing to measurements obtained by the anemometers. The footprint is a positively skewed distribution spread over 10s to100s of meters with a peak at the location of the dominant flux source. For this study, the footprint was estimated using Kljun et al. (2015) which identifies the origin of the flux by employing a backward Lagrangian stochastic particle dispersion model that traces particles in reverse from the measurement point to their original source location. The Kljun et al. (2015) model was developed for terrestrial applications and doesn't account for the dynamic and transitional characteristics of the coastal ocean. It was nonetheless employed here because this is no aquatic alternative. This limitation does not critically impact the objectives of our study which does not require precise localization of the flux source. The footprint is only shared to demonstrate the relative flux distribution and patterns to provide context to the results. The model is run using measurement height, wind speed, Obukhov Length, friction velocity, roughness length, and boundary layer height. All variables were determined from the anemometers except boundary layer height which was set to 750 m because it is a good approximation for this environment (Lavers et al. 2019). Altering the boundary layer height negligibly impacted the footprint.

We represent the footprint as a discrete variable defined by the distance between the anemometer and the footprint peak as shown in Fig. 4. The median flux peak is 138 m, 197 m, 265 m and 338 m from the beach tower at the respective anemometer heights of 14.4, 18.4, 22.4 and 26.4 m, respectively. All footprint peaks are significantly different. The results here nicely illustrate why the requirements of MOST are expected to be violated nearshore. Fluxes measured at a single location but different heights each correspond to energy exchange originating from distinct upwind surface regions. These measurements reflect the spatially resolved contribution of surface fluxes. In cases where the underlying surface is uniform, fluxes are expected to remain consistent across heights. However, when the surface is heterogeneous, flux variance with height is expected, indicating that the flux layer is not uniform. Recalling that the beach tower is about 40 m from the mean water line, the median primary flux source location ranges from about 90 to 290 m from shore. This corresponds to depths of 2.5 to 5 m, a region where wave characteristics, including height, steepness, speed, breaking, and direction, all change rapidly. We also note that the flux footprint includes a horizontal crosswind component which isn't quantified here but further increases heterogeneity.

https://doi.org/10.5194/wes-2026-21
Preprint. Discussion started: 12 February 2026

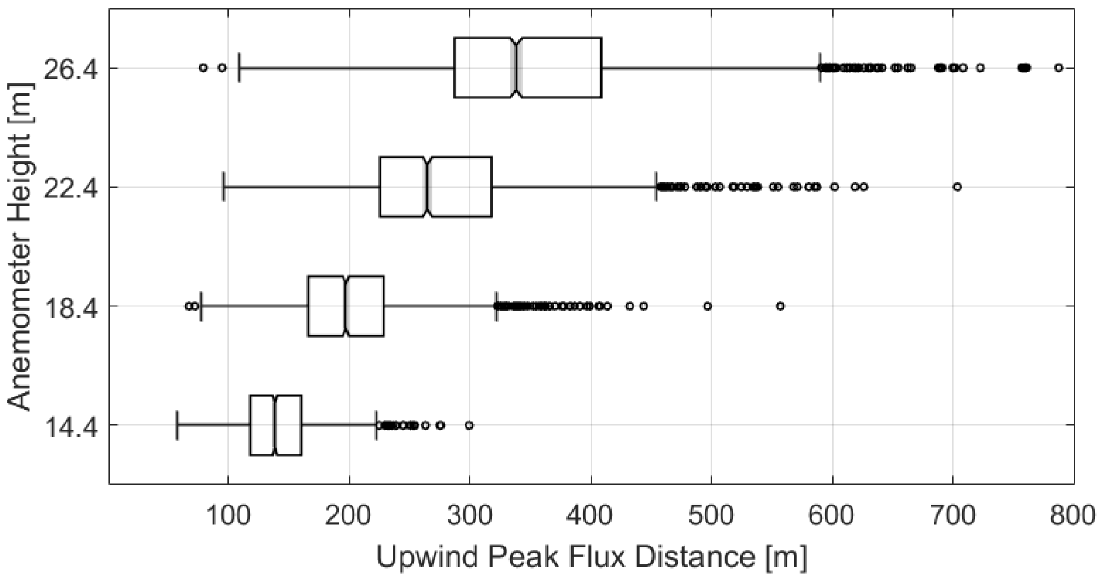

Figure 4. Upwind distance to the peak of the flux footprint for each anemometer. In each box the center line and notches show the median and 95% confidence intervals, and the edges are the 25th and 75th percentiles. Approximately 99.3 % of the data lies within the whiskers, and the circles are outliers.

4 Results

4.1 Wind and Flux Profiles

The winds during the experiment generally were calm. Mean U = 6.9 m s^{-1}, median U = 6 m s^{-1}. The maximum wind speed was U = 19 m s^{-1} but only 67 runs (~1.5 days) had wind speed above 15 m s^{-1}. Figure 5 shows profiles of wind speed, friction velocity, and normalized friction velocity. The wind increases about 0.8 m s^{-1} between 14.5 and 26.4 m. Evidently, the friction velocity is not constant but decreases with height. In the mean, u_* decreases 15% between 14.4 and 26.4 m despite increasing wind speeds. We can account for the impact of wind speed on the friction velocity by normalizing u_* by U_z. Results show that the normalized friction velocity decreases 21% with height over the profile. The profiles become increasingly intriguing when separated into directional bins, as shown in Fig. 6 where the change in u_* and U_z from 14.4 m are shown. Between 14 and 18 m the friction velocity is unchanged for onshore winds, decreases slightly for oblique wind, and decreases rapidly for alongshore wind. At 22 m, friction velocities relative to 14 m converge to an approximate common value. At 26 m, change in u_* from 14 m is largest for onshore wind and lower for oblique and alongshore winds. All profiles show wind speed increases with height. This is most pronounced during alongshore winds and least during onshore. Between 14.4 m and 26.4 m mean U_z change is 0.44 m s^{-1}, 0.72 m s^{-1}, and 1 m s^{-1} for onshore, oblique, and alongshore winds, respectively.

https://doi.org/10.5194/wes-2026-21
Preprint. Discussion started: 12 February 2026

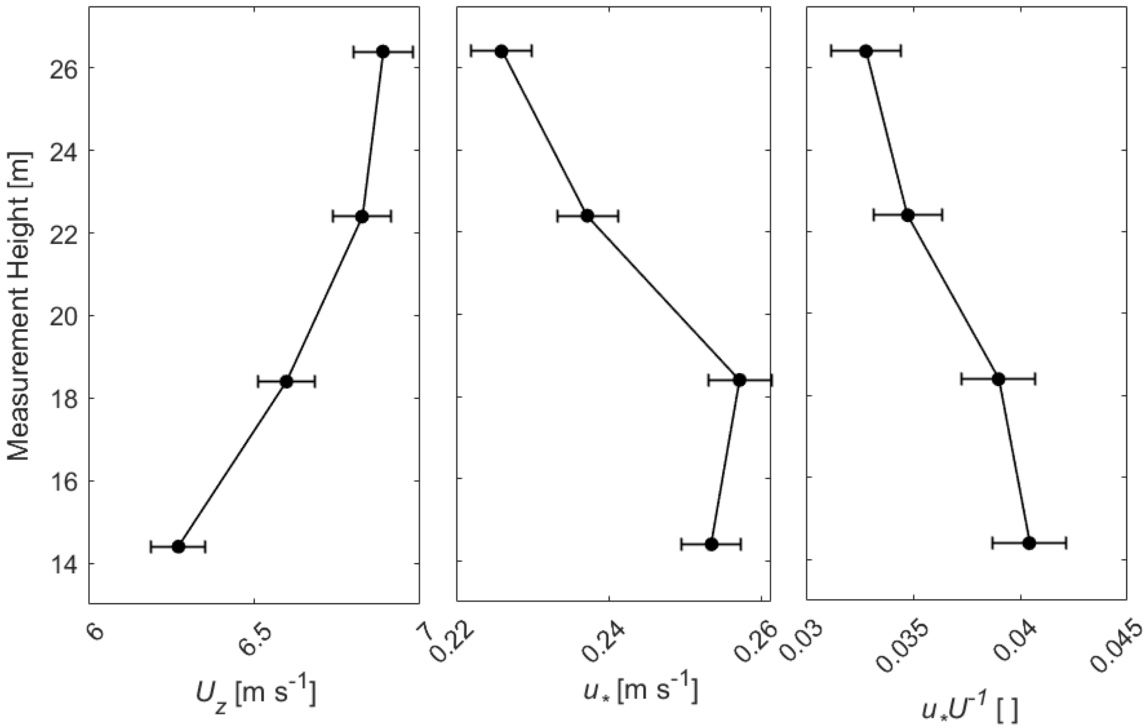

Figure 5. Mean profiles of wind speed, friction velocity, and normalized friction velocity. Horizontal bars are 95% confidence intervals.

https://doi.org/10.5194/wes-2026-21
Preprint. Discussion started: 12 February 2026

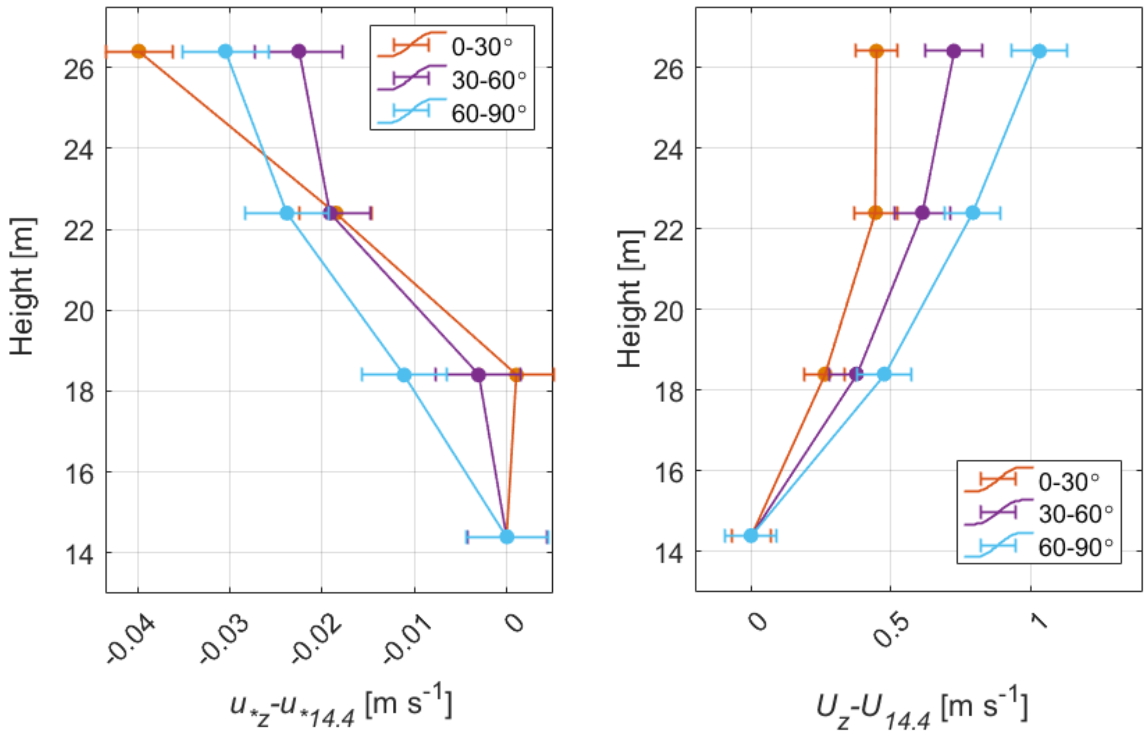

Figure 6. Mean profiles of friction velocity and wind speed. The profiles are separated by wind direction, and each shows the difference between the measurement at that height and the measurement at 14.4 m. Horizontal bars are 95% confidence intervals of the mean.

4.2 Wind and Flux Gradients

We can further investigate the boundary layer structure by exploring the gradients of wind and momentum. Figure 7 shows cumulative densities of wind speed and friction velocity differences between successive heights. Generally, wind speed increases with height. A closer look exposes many nuances. For example, alongshore wind speeds always increase with height, whereas oblique and onshore winds often increase with height. Notable exceptions occur between 22 and 26 m for onshore and oblique winds which *decrease* with height 75% and 38% of the time, respectively, and onshore between 18 and 22 m where wind speeds decrease about 28% of the time. Wind speeds increase most rapidly when the wind is alongshore and least when onshore. Regardless of direction, wind speed gradients are largest nearer the surface and decrease aloft. For friction velocity, Δu_* is negative for at least 90% of runs. This means the friction velocity almost always decreases with height. The two exceptions occur between 14 and 18 m during onshore and oblique winds when Δu_* is positive 40% and 20% of the time, respectively.

https://doi.org/10.5194/wes-2026-21
Preprint. Discussion started: 12 February 2026

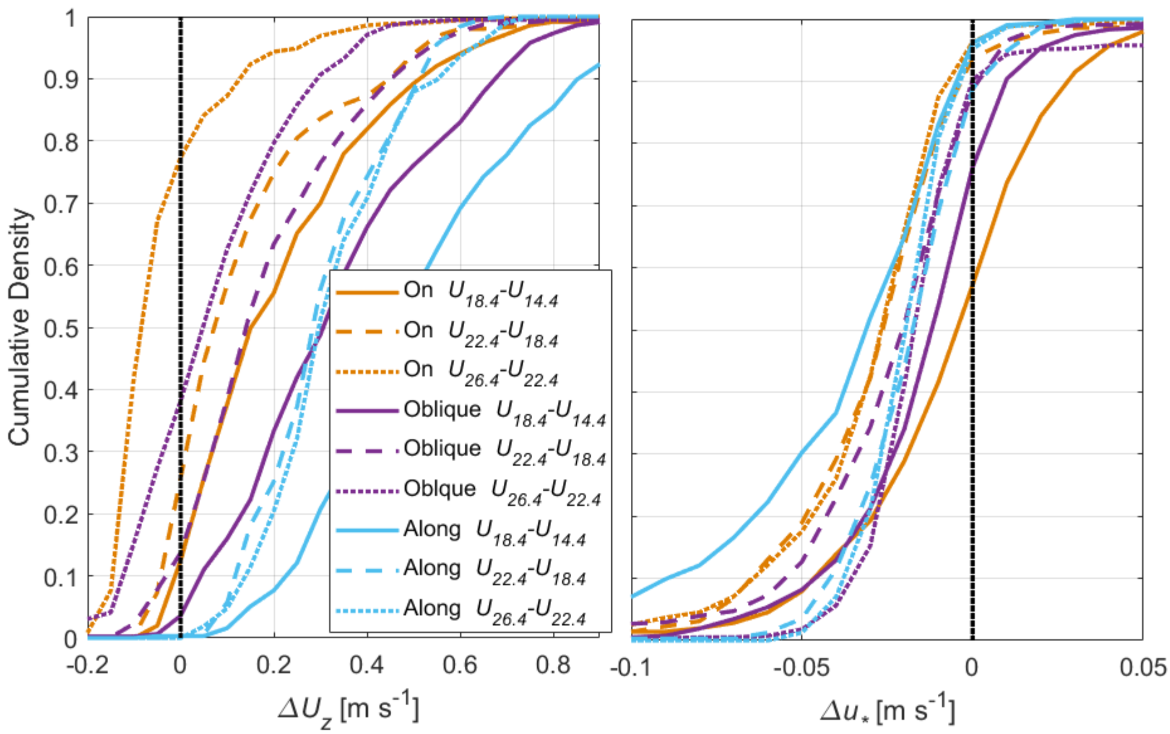

Figure 7. Cumulative density function for change in wind speed (left) and friction velocity (right) between successive heights. The lines, orange for onshore wind, purple for oblique, and blue for alongshore wind, are further divided by height.

5 Discussion

5.1 The Divergent Flux Layer

Results indicate that the flux layer does not vary with height. However, even a constant flux layer has natural variability, and so a more nuance approach is needed. To this end we follow two methods. The first was to apply a least squares regression to each of the 1448 runs, followed by a t-test on the regression slope. Results showed that the slope of the friction velocity is significantly different from zero (i.e., the flux is divergent) most of the time. The outcomes, in Fig. 8, are coloured based on confidence, and show 23% of runs are divergent at $p \leq 0.05$, 38% are divergent at $p \leq 0.10$, and 68% of profiles are divergent at $p \leq 0.25$. These results are robust despite the challenge of achieving statistical significance with the small sample size for each profile ($n = 4$). The second method for evaluating the flux layer follows the methodology in Ortiz-Suslow et al. (2021) who followed a procedure like Mahrt et al. (2018). They also used a linear model to determine the slope of the flux gradient with respect to height but went on to compare it to a maximum allowable ± 10% flux gradient from the median height

https://doi.org/10.5194/wes-2026-21
Preprint. Discussion started: 12 February 2026

of the profile. This is justified because the flux layer is inherently variable, so a somewhat arbitrary gradient threshold is used to assess whether flux changes with height are small enough to consider the profile constant. For each of 1448 profiles, the regression provides an observed slope $m_o = \Delta u_*/\Delta z$ and an expected slope following

$$m_e = \frac{0.2u_*}{\Delta z}, \quad (6)$$

where u_* is the mean friction velocity for the individual run. The slope index is then determined using

$$m_r = \frac{m_e - m_o}{m_e}. \quad (7)$$

Here, the signs of m_e and m_o are aligned. When $m_r > 0$ the profile is classified as constant and when $m_r < 0$ the profile is classified as divergent within the prescribed tolerance. The lower and upper bounds of m_r are $-\infty$ and 1 which occur when $m_o \rightarrow \infty$ and $m_o \rightarrow 0$, respectively. The results in Fig. 9 show that divergent flux occurs 69% of the time for onshore winds, 50% for oblique winds, and 57% for alongshore winds. These results are largely consistent with the former method and affirm that most coastal flux profiles are not constant.

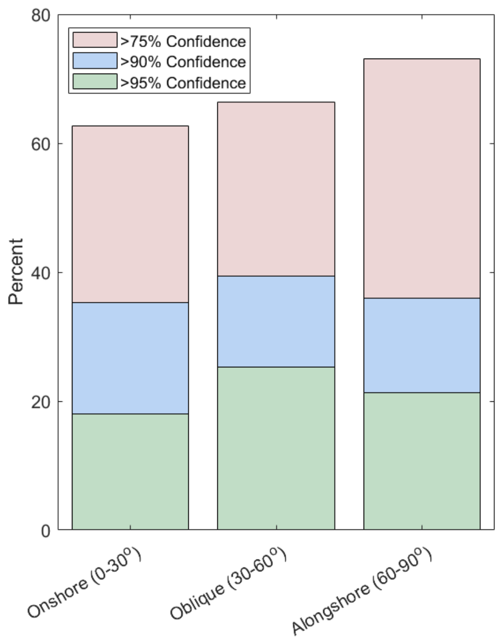

Figure 8. Percentage of flux profiles that are divergent (i.e., not constant) at different confidence levels for onshore, oblique, and alongshore winds.

https://doi.org/10.5194/wes-2026-21
Preprint. Discussion started: 12 February 2026

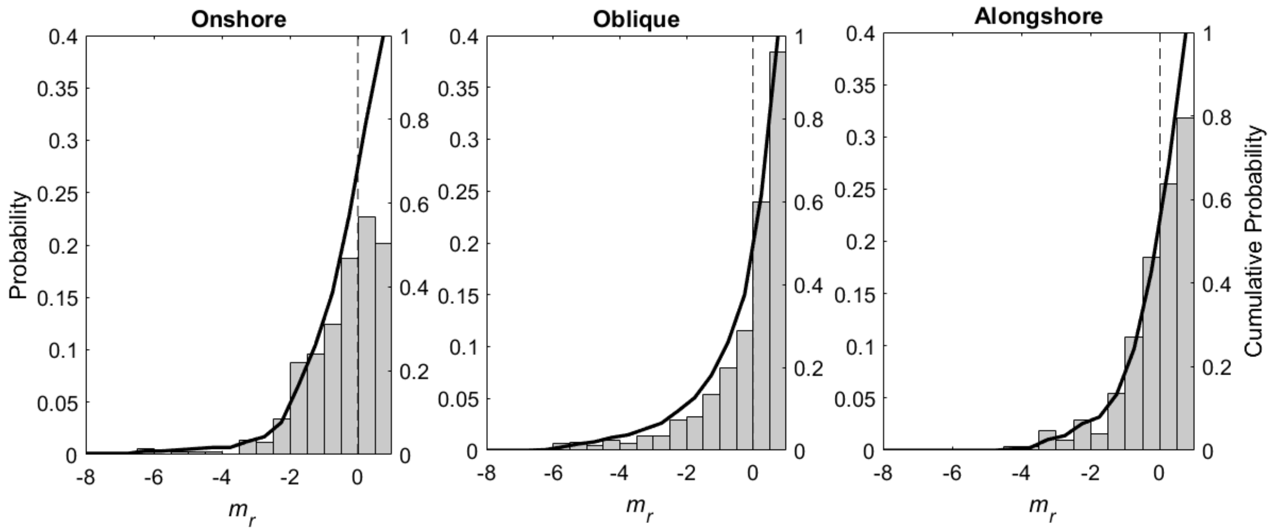

Figure 9. Probability distribution (bar chart) and cumulative density (solid black line) of the slope index m_r classified by wind direction. In each subplot the dashed vertical line at m_r = 0 is the demarcation between divergent (m_r < 0) and constant (m_r > 0) flux layers.

Our results, which show ~38% of flux gradients are constant, are very similar to Ortiz-Suslow et al. (2021) who found 30-40% of profiles constant. This is surprising because their measurements were made in the open ocean which has greater homogeneity than the coast. Notwithstanding, combining our results with Ortiz-Suslow et al. (2021) observations between 3 and 16 m, reveals a propensity toward divergent flux in the marine environment between the surface and 26 m. Figure 10 is a plot of m_r as a function of U_z that shows the flux layer tends to become more constant as wind speed increases. The flux profile is most likely to be divergent for $U_z < 8$ m s^{-1} which accounts for 72% of this data. The same general trend exists when looking at each wind direction category independently, which are not significantly different from each other (not shown). Ortiz-Suslow et al. (2021) found m_r increased only up to 4 m s^{-1} and no wind speed dependence beyond that, though they did identify mean m_r > 0 briefly during 14 m s^{-1} associated with an atmospheric front.

Many winds above 8 m s^{-1} are oblique and alongshore (recall Fig. 3) which may contribute to the slightly higher rate of constant flux for this wind direction. Typically, an increase in wind speed increases friction velocity, which means the atmosphere is moving from neutrality as the absolute value of the Obukhov Length increases (Eq. 4). It is therefore reasonable

https://doi.org/10.5194/wes-2026-21
Preprint. Discussion started: 12 February 2026

to think the increase in m_r at higher winds in Fig. 10 may reflect stability changes. But this isn't the case. We found no evidence that a neutral boundary is more likely to yield a divergent flux layer. In fact, recreating Fig. 9 categorized by stability (Fig. 11) shows the opposite. Seventy-seven percent of flux profiles are divergent for stable conditions (383 runs), 58% for unstable (706 runs), and only 35% for neutral conditions (359 runs). We also plotted ζ as a function of wind direction, m_r as a function of ζ, and ζ as a function of wind speed, all in Fig. A1. These show: 1) higher winds speed yield neutral condition, 2) m_r is not stability dependent, and 3) there is a very slight but statically significant trend toward atmospheric neutrality as winds shift parallel to shore. The 95% confidence intervals of ζ are [$-0.32 < \zeta < -0.24$] onshore, [$-0.19 < \zeta < -0.11$] oblique, and [$-0.08 < \zeta < -0.02$] alongshore. Therefore, any observed link between wind direction and the presence of a constant flux layer cannot be explained by changes in atmospheric stability.

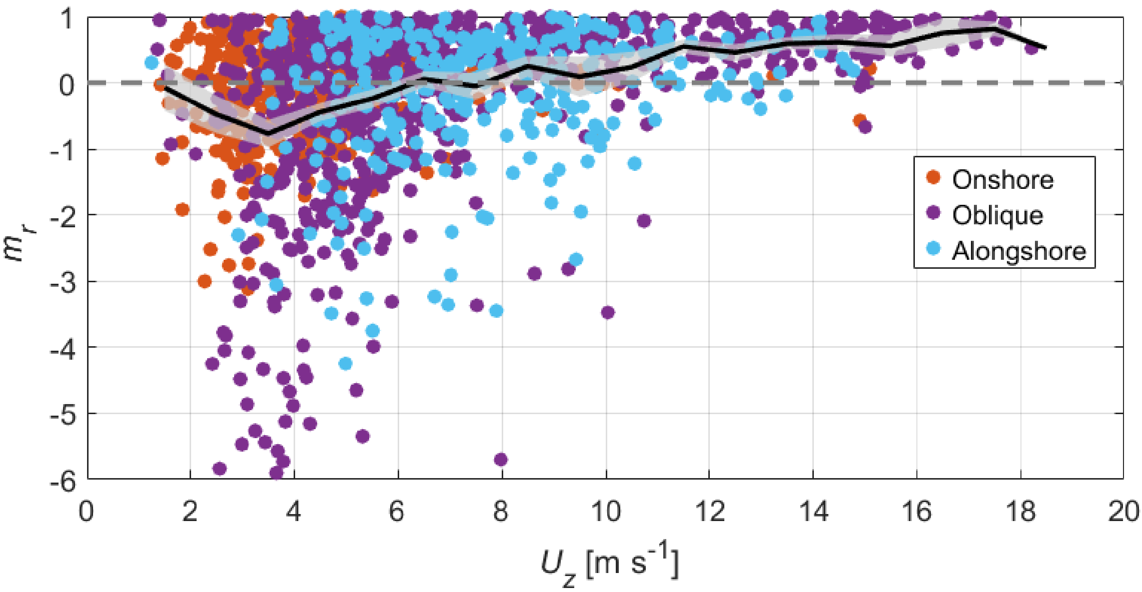

Figure 10. Slope index (m_r) as a function of mean wind speed (U_z). Data are coloured for onshore, oblique, and alongshore wind. The black line is the mean in 1 m s^{-1} bins with 95% confidence interval shaded area.

https://doi.org/10.5194/wes-2026-21
Preprint. Discussion started: 12 February 2026

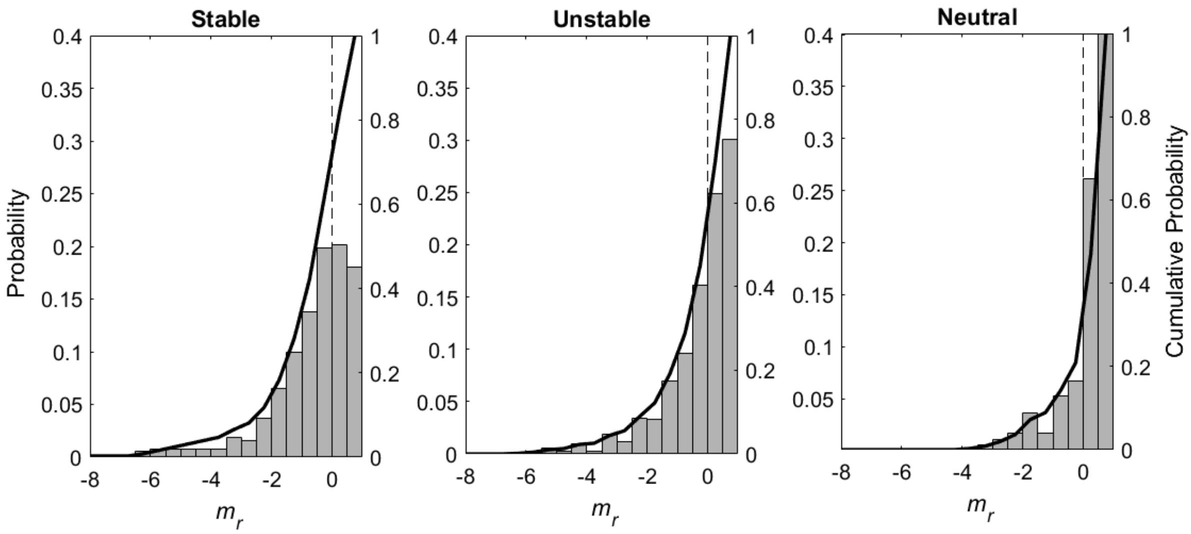

Figure 11. Probability distribution (bar chart) and cumulative density (solid black line) of the slope index m_r classified by atmospheric stability. In each subplot the dashed vertical line at m_r = 0 is the demarcation between divergent (m_r < 0) and constant (m_r > 0) flux layers.

5.2 Stability Gradient Functions

Despite the absence of a constant flux layer and corresponding lack of strict adherence to similarity theory, we nonetheless computed the dimensionless functions to characterize the flow behaviour. This is necessitated by the fact that we don't have a suitable alternative to the gradient functions that have long been applied. The absence of strict similarity does not preclude the use of dimensionless analysis; rather, it demands a more nuanced approach that accounts for the influence of divergent flux profiles that exist in the ocean-to-land transition zone. The wind shear was calculated from the least squares fit of U as a function of $ln(z)$, including $U = 0$ at $z = 0$, using a second order polynomial. And ζ was computed for each height by applying observed values to Eq. 3. Finally, $\Phi_u(\zeta)$ was calculated for every height and every profile using the conventional κ = 0.41. Means in bins of ζ = 0.1 were fit using functions $\Phi_u(\zeta) = A + B(\zeta)$ for $\zeta > 0$ and $\Phi_u(\zeta) = [a - b(\zeta)]^c$ for $\Phi_u(\zeta) < 0$, consistent with the fits adopted by Kitaigorodskii and Donelan (1984) and others. In most cases we fit the data over the range of -2 to 2, the exception is alongshore wind which we truncated the fit for $\Phi_u(\zeta) < 0$ at -1 because we lack sufficient data beyond this value. In every case, more extreme values also have significant scatter and would add large uncertainty to the fits

https://doi.org/10.5194/wes-2026-21
Preprint. Discussion started: 12 February 2026

if they were extended beyond our assigned limits. Results are in Fig. 12 and Table 1. Note that we repeated this entire process using only the observed data (i.e., not including $U = 0$ at $z = 0$) and found the results were very similar to those presented here.

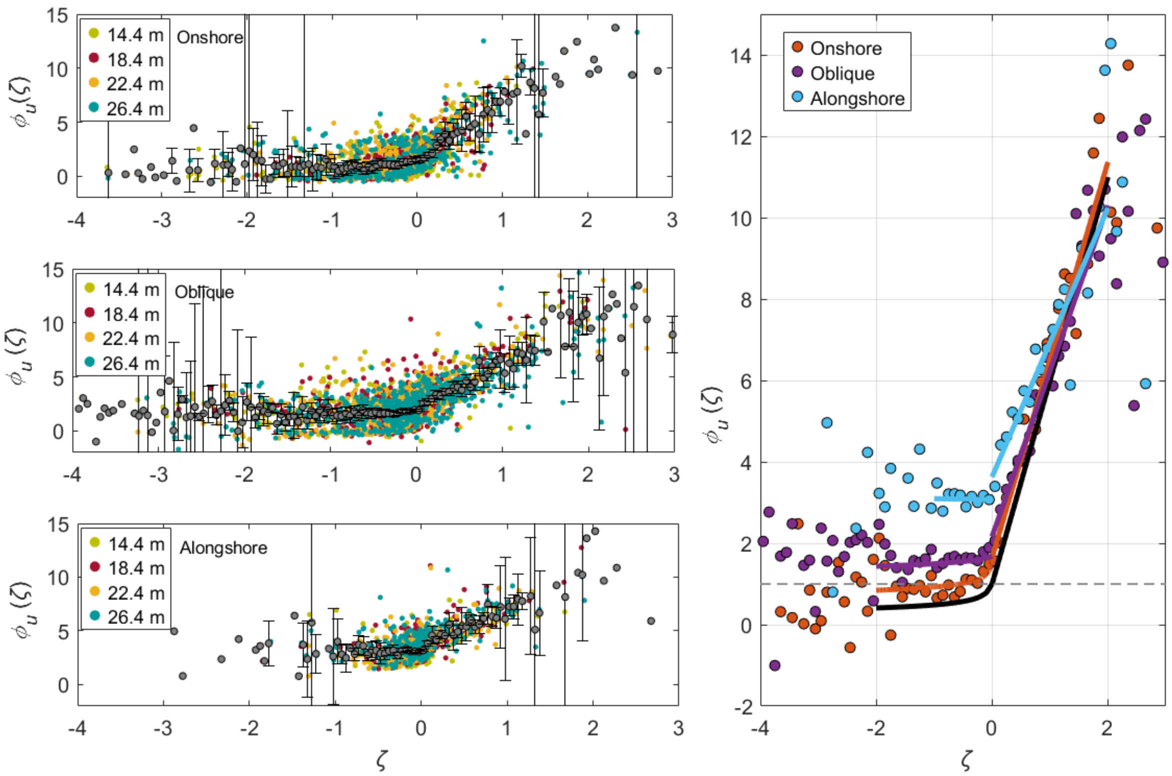

300 **Figure 12. Stability corrections calculated by solving $\Phi_u(\zeta) = \frac{u_*}{\kappa z}\left(\frac{\partial U}{\partial z}\right)$, where $\zeta = z/L$. The left three panels from top to bottom are for onshore, oblique, and alongshore winds. Colors show the measurement height used for u_* and ζ, and grey dots with whiskers show the binned means and 95% confidence intervals. The mean values are also plotted on the right panel and fitted with lines as described in the text. The black lines are the stability correction from Kitaigorodskii and Donelan (1984). Please note that many data points are plotted behind others.**

305

Table 1. Equations of fit for stability functions following the conventional $\Phi_u(\zeta) = A + B(\zeta)$ for $\zeta > 0$ and $\Phi_u(\zeta) = [a - b(\zeta)]^c$ for $\Phi_u(\zeta) < 0$.

	Kitaigorodskii and Donelan (1984)	Onshore	Oblique	Alongshore

https://doi.org/10.5194/wes-2026-21
Preprint. Discussion started: 12 February 2026

$(\zeta) < 0$	$1 - 17(\zeta)^{-1/4}$	$[0.015 - 1.81(\zeta)]^{-0.13}$	$[-0.0003 + 0.0015(\zeta)]^{-0.0673}$	$[1.4 - 0.0031(\zeta)]^{3.3}$
$(\zeta) > 0$	$1 + 5(\zeta)$	$1.6 + 5(\zeta)$	$2.1 + 4.2(\zeta)$	$3.6 + 3.3(\zeta)$

Figure 12 shows that $\Phi_u(\zeta)$ is generally highest for any given ζ during alongshore winds and lowest for onshore. Alongshore and oblique winds are both higher than Kitaigorodskii and Donelan (1984), however, the 95% confidence interval for $\Phi_u(\zeta)$ for onshore winds encompass the fit from Kitaigorodskii and Donelan (1984) so they are not significantly different. This is illustrated in Fig. B1 which shows the left side of Fig. 12 in greater detail with the Kitaigorodskii and Donelan (1984) fit overlaid. Differences can be further quantified by investigative $\Phi_u(\zeta)$ relative to stability. To do so, we define $-0.05 \le \zeta \le 0.1$ as neutral conditions, $\zeta \ge 0.1$ for a stable boundary layer, and when $\zeta \le -0.05$ for unstable. The sign of ζ is dictated by heat flux in the denominator of Eq. 4. During neutral conditions the gradient function is expected to become obsolete, i.e., $\Phi_u(0) = 1$. This is achieved through the von Kármán constant in Eq. 3, the reported limits of which are in the approximate range of $\kappa = 0.37$ (Bregmann, 1998) to $\kappa = 0.43$ (Andreas et al., 2006), with $\kappa = 0.41$ frequently adopted. The result from Kitaigorodskii and Donelan (1984) in Fig. 12 shows that in the open ocean when the atmosphere is neutral, the scaling parameter neither enhances nor diminishes the velocity profile. For our data neutral conditions do not result in $\Phi_u(0) = 1$. For each wind direction the value was taken as the mean of the intercepts for stable and unstable conditions. They are $\Phi_u(0) = 1.65$ onshore, $\Phi_u(0) = 1.9$ oblique, and $\Phi_u(0) = 3.35$ alongshore (Fig. 12 right panel). For onshore winds, the intercepts were very similar, for other directions they had greater spread. In neutral conditions these data therefore show the wind speed increases with height more rapidly than in typical ocean conditions. This is most predominant when the wind is alongshore and less for onshore when $\Phi_u(0)$ approaches one. To shift the data so that $\Phi_u(0) = 1$, the von Kármán constant in Eq. 3 must be altered to $\kappa = 0.28$, $\kappa = 0.2$, and $\kappa = 0.12$ for onshore, oblique, and alongshore conditions respectively. The von Kármán constant appears in the denominator of the Eq. 4 for the Obukhov Length so reducing κ effects the magnitude of L and nudges ζ towards neutral conditions. This result does not suggest a reevaluation of the von Kármán is necessary. Rather, it highlights the challenge of applying this conventional method when non-uniform roughness distorts both the flux gradient and the velocity profile.

Notwithstanding the large variability in $\Phi_u(\zeta)$ for neutral conditions, each stability correction follows similar and recognizable trends that track with Kitaigorodskii and Donelan (1984) and other empirical results. When conditions are unstable ($\zeta \le -0.05$), $\Phi_u(\zeta)$ generally decreases slowly as the atmosphere becomes instability increases, and when conditions are stable ($\zeta \ge 0.1$) $\Phi_u(\zeta)$ increases rapidly with stability. Some cursory evidence suggests that for alongshore, stable conditions $\Phi_u(\zeta)$ increases slower than the others, but the slopes are not significantly different. Finally, we note that these results are independent of the measurement height or friction velocity used. For each wind profile, Eq. 3 was solved for every z and corresponding values

https://doi.org/10.5194/wes-2026-21
Preprint. Discussion started: 12 February 2026

for u_* and ζ. All resulting values of $\Phi_u(\zeta)$ are plotted in Fig. 12, i.e., every profile is represented four times for each of the four measurement heights. This inevitably adds scatter to Fig. 12, not least because the flux layer is very often not constant. Nonetheless, isolating the measurements and creating multiple iterations of Fig. 12 using each of the heights individually, i.e., every profile is represented just once using z, u_*, and ζ from a single height, the outcome is largely unchanged. In other words, the results in Fig. 12 are independent of the height measurement chosen.

In summary, two notable elements are revealed in Fig. 12. First is that coastal wind speed gradients at this location are generally steeper than observed offshore. Second is that the wind speed increases with height more rapidly when the wind direction is aligned with the shoreline, compared to when it is onshore, as reflected in Fig. 6. These are discussed below.

5.3 Coastal Winds

The research site at Duck, North Carolina has a modest ~6 m dune (Brodie et al., 2019). When wind encounters a coastal barrier such as a dune, the atmospheric response is the formation of a pressure ridge, known as damming (Overland and Bond, 1993). Damming can cause wind to accelerate and shift direction, and it is possible that such effects played a role in shaping the wind profile at this stie. He et al. (2021) observed wind turning at a land-sea interface, resulting in a dominant wind direction aligned parallel to the coastline and acceleration in wind speed which they ascribe to lateral, orographic boundary near the land-sea transition region. Schumann and Martin (1991) also attributed fast coastal winds to topographic acceleration by land. Using years of QuikSCAT satellite data, Liu et al. (2008) found regions of high wind power energy associated with acceleration of winds due to wind channelling by land topography. Taken together, these studies demonstrate that wind acceleration along the coast is expected, leading to notable changes in wind speed profiles. However, several studies on aeolian transport have shown that wind acceleration is most pronounced during onshore flow when compared to alongshore. For instance, Schwarz et al. (2020) observed that wind speeds increased by a factor of three from the base to the crest of a foredune, with the strongest acceleration occurring during onshore winds. This pattern aligns with findings by Hesp et al. (2015) who also noted enhanced acceleration when winds approached within 30° perpendicular to the coast. Similarly, Bauer et al. (2012) reported that the increase in wind speed from the dune foot to the crest was greatest under onshore wind conditions. Our results show wind profiles have greatest shear during alongshore winds. While the dune at the site is likely contributing to the overall wind structure through terrain-induced acceleration it cannot fully account for the directional dependence of shear. The pronounced increase in shear during alongshore flow implies that additional factors impact the profiles of wind at this location.

5.4. Slanting-Fetch

At a coastal location, Ardhuin et al. (2007) found that the wind sea portion of the wave spectrum adheres to established growth curves for significant wave height and peak period during onshore wind conditions. However, this relationship did not hold for alongshore winds. Under these conditions, often referred to as slanting-fetch, waves continue to develop preferentially in

https://doi.org/10.5194/wes-2026-21
Preprint. Discussion started: 12 February 2026

Wind Energy Science Discussions

the onshore direction despite the wind originating from a different angle. Onshore winds promote strong wind-wave coupling due to extended spatial and temporal interaction scales whereas alongshore winds have very low effective fetch, resulting in weaker wind-wave coupling. Potter et al. (2022) and Shabani et al. (2016) both attributed this mechanism to their measurements of higher momentum flux for onshore winds compared to alongshore independent of wind speed.

Waves refract as they shoal, becoming progressively aligned with the coast. For winds that are not onshore, this leads to increased wind-wave misalignment and decreased effective fetch as waves approach land. This means the slanting-fetch effect should rise as depth shallows. This is represented in Fig. 13 which shows box plots of normalized friction velocity u_*/U_z for each wind direction and measurement height. Using the normalized friction velocity allows us to examine trends while controlling for winds speed. For each height, the friction velocity decreases as wind-wave misalignment increases. For each direction, friction velocity decreases with height. The highest three u_*/U_z are onshore at 14, 18, and 22 m, respectively, which are all significantly different from each other and everything else, and a clear indication of the slanting-fetch effect. Onshore at 26 m is the fourth highest u_*/U_z tied with 14 m for oblique and alongshore winds. This shows that, in shallow water, when account for wind speed, fluxes recorded at 26 m (~5 m depth) during onshore winds are approximately equal to those recorded at 14 m (~2.5 m depth) for oblique and alongshore winds. The lowest flux in Fig. 13 is found at 26 m alongshore wind, which is significantly lower than all others. The normalized friction velocity for alongshore wind at 26 m u_*/U_z = 0.026, is about half the value for 14 m onshore wind, u_*/U_z = 0.047. Hence a doubling of friction velocity is possible when accounting for wind speed and direction. Fig. 13 also shows the converging of u_*/U_z as measurement height increases, highlighting the decreasing effect of slanting-fetch as depth increases.

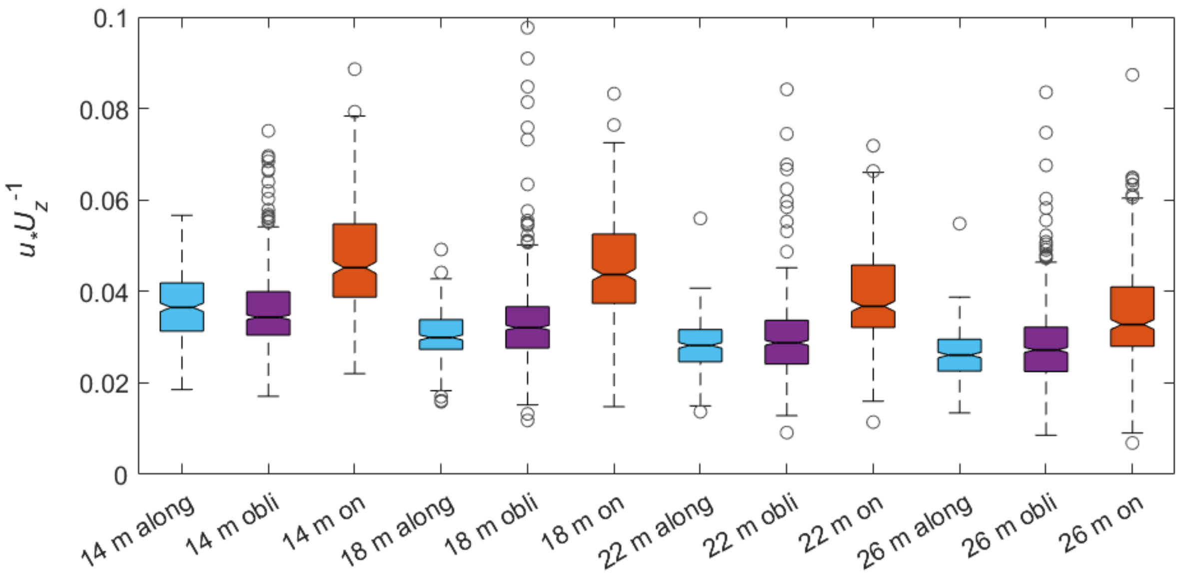

https://doi.org/10.5194/wes-2026-21
Preprint. Discussion started: 12 February 2026

Figure 13. Normalized friction velocity for every height and wind direction category. Blue boxes are alongshore winds, purple are oblique winds, and red are onshore winds. Each direction is represented once for each measurement height. For each box, the centre line is the median and the notches are the median 95% confidence intervals. The top and bottom edges are the 75th and 25th percentiles, ~99.3 % of the data lie within the whiskers, and circles are outliers.

We propose that the changes in the friction velocity due to wind-wave misalignment are propagated through the boundary layer impacting wind speed. According to Eq. 5 the friction velocity increases with wind speed. However, because nearshore surface roughness increases due to wave shoaling independent of the wind, the friction also modulates the wind speed. Hence, elevated nearshore drag during wind-wave alignment gives rise to a decrease in wind speed. In other words, the shorter effective fetch during onshore winds relative to alongshore creates an effectively rougher surface which drags and slows the wind. Decrease in wind speed due to higher surface friction is most pronounced where the water is shallowest (as observed at 14 m) and least pronounced offshore in the deepest water (as observed at 26 m), also shown in Fig. 6. The slowing of wind near the surface due to friction propagates through the boundary layer reducing wind speed because less momentum is transferred upward. Additional studies are needed to fully understand the wind speed profile above 26 m, particularly up to turbine hub height. However, many terrestrial studies have demonstrated how winds aloft respond to changes in surface roughness. Terrestrial stilling is a well-documented trend of decreasing wind speeds over land largely due to land cover change including urbanization (e.g., Wang et al., 2020, Li et al., 2018) and afforestation (e.g., Wever, 2012). Decline of near-surface wind speed can propagate through the boundary layer decreasing speed to over 5 km (Luu et al., 2023). Near the surface, the upward propagation of momentum should be least during stable conditions when vertical motion is suppressed, and largest during unstable conditions when buoyant and shear-driven mixing enhance vertical momentum transport accelerating winds aloft. In our case, unstable conditions occurred 54% of the time, natural 25%, and stable 21%. Recall however that atmospheric instability was greatest for onshore wind and least for alongshore whereas winds speed gradients were greatest for alongshore and least for onshore. While a tendency toward instability may have contributed to the elevated wind gradients observed, it does not explain why gradients differ by wind direction.

6 Summary and Final Remarks

In this study, over seven hundred hours of sonic anemometer data collected simultaneously at four heights on a beach tower were used to explore wind speed and turbulence profiles along the coast. The anemometers were arranged from 14 to 26 m above the mean water surface resulting in sequential and overlapping flux footprints that covered the heterogenous inner shelf extending about 600 m from shore. The data were separated based on their wind direction relative to shore (onshore ± 30°, oblique ± 30-60°, alongshore ± 60- 90°). The boundary layer was found to be divergent (non-constant) ~60% of the time. A constant flux layer was most common for winds above 8 m s^{-1}, during oblique winds, and during neutral atmospheric stability, but no relationship between these was found. We calculated the stability corrections following Monin-Obukhov Similarity Theory (Monin and Obukhov, 1954) and found the wind speed gradient is highest during alongshore winds and lowest during

https://doi.org/10.5194/wes-2026-21
Preprint. Discussion started: 12 February 2026

onshore. This occurs because waves refract and shoal parallel to shore which increases surface roughness independent of wind. As a result, wind direction dictates the angle at which waves and wind interact. When wind is onshore it travels across the waves resulting in strong wind-wave coupling, when wind is alongshore it travels along the waves and reduces the coupling which decreases the effective roughness. This phenomenon is called slanting-fetch. We determined that changes in the friction velocity in response to wind-wave angle alters the wind speed which then propagated through the boundary layer impacting winds aloft.

In their study of coastal wind gradients, Barthelmie et al. (2007) argue that because the standard roughness length of the ocean, $z_0 \approx 2 \times 10^{-4}$ m, is two orders of magnitude less than the smallest land roughness, found in a grass field, $z_0 \approx 3 \times 10^{-2}$ m (Stull, 2012), even relatively large changes in sea surface roughness have only a small impact on wind speed profile. Our results suggest otherwise. We show that coastal roughness length can vary from $z_0 \approx 2.4 \times 10^{-3}$ m for onshore winds measured at 14.4 m (flux footprint peak ~2.5 m depth) to $z_0 \approx 8.2 \times 10^{-5}$ m alongshore at 26.4 m (flux footprint peak ~5 m depth). This two orders of magnitude difference manifest as large differences in wind speed aloft. Coasts are unique because shallow water causes wave development in the onshore direction leading to waves that are not aligned with the wind yet have wind sea-like characteristics. Such conditions do not occur in deep water, besides tropical cyclones (Manzella et al. 2024, Potter et al., 2015b). Therefore, the applicability of these results elsewhere is contingent upon local bathymetry which dictates the transition of waves to intermediate and shallow water, where they evolve independent of wind.

The average water depth of wind farms constructed in Europe in 2019 is 34 m with several farms much shallower (WindEurope, 2021). In the United States offshore leases for wind energy in the Atlantic have an average depth of 30 m (ICF, 2021) and the Lake Charles lease in the Gulf of Mexico has a depth below 20 m (Fuchs et al. 2023). Waves in these transitional depths shoal and morph, becoming taller, steeper, slower, and more aligned with the coast as they respond to bottom friction. Potter et al. (2022) showed that a doubling of the aerodynamic drag coefficient can occur because of slanting-fetch over transitional waves at depths ~10 m while He et al. (2021) found the surface much smoother for alongshore wind at 20 m compared to onshore. Smith et al. (1980) also reported drag coefficient for alongshore winds much lower than during onshore winds at a 59 m coastal site though didn't ascribe a mechanism. Since flux footprints increase with height, the footprint at hub height encompasses a much larger area than reported here. If recorded at 100 m, the corresponding mean footprint peak for our data would be 1.4 km with a maximum value above 2.7 km. This leads to a range of almost 5.5 km. A distance over which the roughness of the surface is expected to change considerably, altering the wind speed aloft. While the effect is likely to be less than revealed by this study, the impact of wind-wave misalignment is clearly very important to wind speed and turbulence aloft. Resource assessment for wind farms should consider the bathymetry and prevailing wind direction to assess the potential impact of slanting-fetch on velocity profiles.

The results of this coastal wind study are shaped by the distinctive geographic and environmental features of the research site, including its unique ocean wave characteristics. While similar wind and wave patterns may be present in other coastal regions,

https://doi.org/10.5194/wes-2026-21
Preprint. Discussion started: 12 February 2026

the interplay between local wind dynamics and wave behaviour is site-specific, influenced by such factors as shoreline orientation, bathymetry, fetch, and prevailing weather systems. Understanding these localized interactions is especially important for offshore wind energy development where waves can alter wind profiles and affect operational efficiency. To assess how these findings compare to other locations, further research is needed to explore regional variations and their implications for energy infrastructure and the effective transition to renewable energy.

Finally, we must reiterate that the methodology applied in this study, based on the Obukhov Length and Monin-Obukhov similarity theory (Monin & Obukhov, 1954), isn't intended to be applied near shore where conditions are heterogenous. However, adopting MOST remains a practical necessity due to the absence of an alternative. The findings of this study should be interpreted recognizing that the application of MOST in such complex settings introduces uncertainty. There is a pressing need for further research to evaluate the conditions under which similarity theory can be reliably applied nearshore, and to explore whether alternative or modified frameworks could offer more robust representations of turbulent exchange processes in these transitional regions.

https://doi.org/10.5194/wes-2026-21
Preprint. Discussion started: 12 February 2026

Appendix A

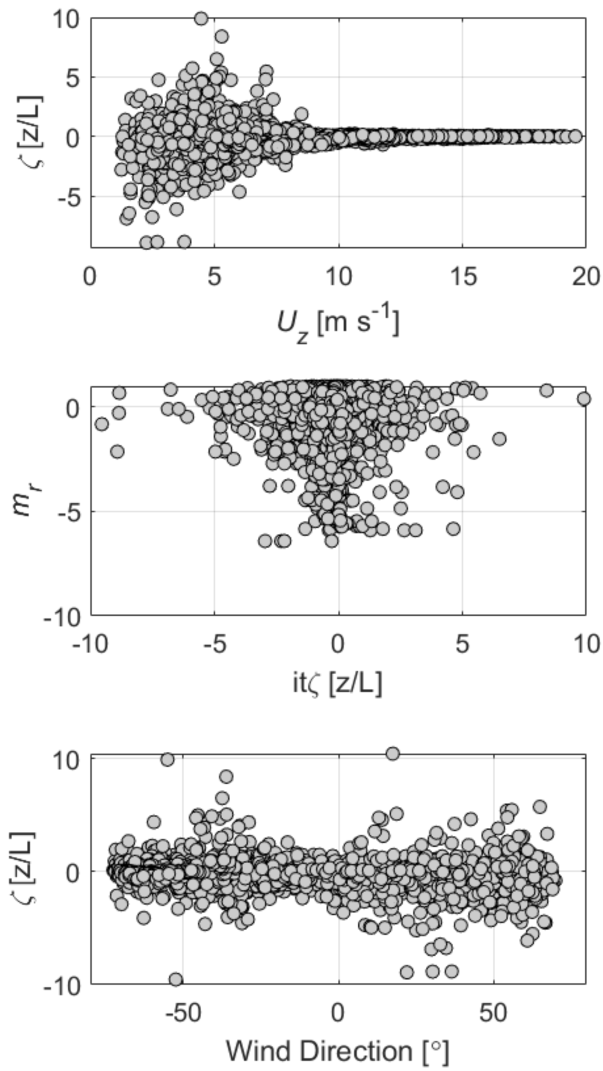

Figure A1. Top: stability as a function of wind speed. Middle: slope index as a function of stability. Bottom: stability as a function of shore-normal wind direction.

https://doi.org/10.5194/wes-2026-21
Preprint. Discussion started: 12 February 2026

Appendix B

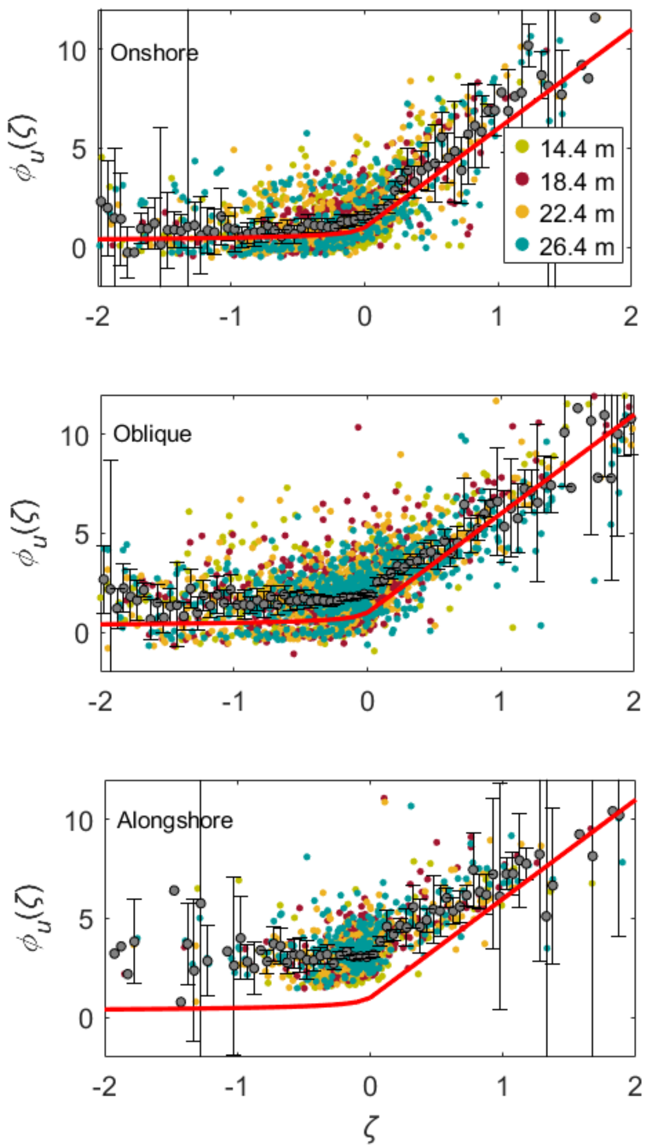

480

Figure B1. Stability corrections as a function of ζ. Colors show the measurement heights and grey dots with whiskers show the binned means and 95% confidence intervals. This figure is like the left side of Fig. 10 but here, the axis limits have decreased and the stability correction from Kitaigorodskii and Donelan (1984) is overlaid in red.

https://doi.org/10.5194/wes-2026-21
Preprint. Discussion started: 12 February 2026

Open Access
WIND ENERGY SCIENCE DISCUSSIONS

Author Contributions

HP conceptualized, executed and managed the experiment, provided resources and acquired funding for the investigation. HP and BE curated the data and completed formal analysis, validation and visualization. HP wrote the original draft of this manuscript which BE reviewed and edited.

Data Availability

The data used in this study are available through The Texas Data Repository at https://doi.org/10.18738/T8/ZYQQ92.

Acknowledgements

Thanks to FRF operations staff who provided invaluable support during the fieldwork and for many months after, and to the science team Dr. Meng Lyu, Dr. Xin Yang, and Robby Haslett.

Financial Support

This research was funded by the National Science Foundation under grant 23319548. Additional support was provided by the Office of Naval Research under grant N00014-24-1-2554.

References

AlSam, A., Szasz, R., & Revstedt, J. (2017). Wind–wave interaction effects on a wind farm power production. *Journal of Energy Resources Technology*, *139*(5), 051213.

Ardhuin, F., Herbers, T. H. C., Watts, K. P., van Vledder, G. P., Jensen, R., & Graber, H. C. (2007). Swell and slanting-fetch effects on wind wave growth. *Journal of Physical Oceanography*, *37*(4), 908-931.

Andreas, E. L., Claffey, K. J., Jordan, R. E., Fairall, C. W., Guest, P. S., Persson, P. O. G., & Grachev, A. A. (2006). Evaluations of the von Kármán constant in the atmospheric surface layer. *Journal of Fluid Mechanics*, *559*, 117-149.

Barthelmie, R. J., Badger, J., Pryor, S. C., Hasager, C. B., Christiansen, M. B., & Jørgensen, B. H. (2007). Offshore coastal wind speed gradients: Issues for the design and development of large offshore windfarms. *Wind Engineering*, *31*(6), 369-382.

Bauer, B. O., Davidson-Arnott, R. G., Walker, I. J., Hesp, P. A., & Ollerhead, J. (2012). Wind direction and complex sediment transport response across a beach–dune system. *Earth Surface Processes and Landforms*, *37*(15), 1661-1677.

Beljaars, A. C. M., & Holtslag, A. A. M. (1991). Flux parameterization over land surfaces for atmospheric models. *Journal of Applied Meteorology and Climatology*, *30*(3), 327-341.

Bilgili, M., & Alphan, H. (2022). Global growth in offshore wind turbine technology. *Clean Technologies and Environmental Policy*, *24*(7), 2215-2227.

Bergmann, J. C. (1998). A physical interpretation of von Kármán's constant based on asymptotic considerations—A new value. *Journal of the atmospheric sciences*, *55*(22), 3403-3407.

https://doi.org/10.5194/wes-2026-21
Preprint. Discussion started: 12 February 2026

Brodie, K., Conery, I., Cohn, N., Spore, N., & Palmsten, M. (2019). Spatial variability of coastal foredune evolution, part a: Timescales of months to years. *Journal of Marine Science and Engineering*, *7*(5), 124.

Businger, J. A., Wyngaard, J. C., Izumi, Y., & Bradley, E. F. (1971). Flux-profile relationships in the atmospheric surface layer. *Journal of Atmospheric Sciences*, *28*(2), 181-189.

Chen, X., Hara, T., & Ginis, I. (2020). Impact of Shoaling Ocean Surface Waves on Wind Stress and Drag Coefficient in Coastal Waters: 1. Uniform Wind. *Journal of Geophysical Research: Oceans*, *125*(7), e2020JC016222.

Costoya, X., DeCastro, M., Carvalho, D., Feng, Z., & Gómez-Gesteira, M. (2021). Climate change impacts on the future offshore wind energy resource in China. *Renewable Energy*, *175*, 731-747.

Courtney, M. S., & Hasager, C. B. (2016). Remote sensing technologies for measuring offshore wind. In *Offshore Wind Farms* (pp. 59-82). Woodhead Publishing.

Drennan, W. M. (2006). On parameterizations of air–sea fluxes. *WIT Transactions on State-of-the-art in Science and Engineering*, *23*.

Dyer, A. J., & Hicks, B. B. (1970). Flux-gradient relationships in the constant flux layer. Quarterly Journal of the Royal Meteorological Society, 96(410), 715-721.

Edson, J. B., Jampana, V., Weller, R. A., Bigorre, S. P., Plueddemann, A. J., Fairall, C. W., ... & Hersbach, H. (2013). On the exchange of momentum over the open ocean. *Journal of Physical Oceanography*, *43*(8), 1589-1610.

Fairall, C. W., Bariteau, L., Grachev, A. A., Hill, R. J., Wolfe, D. E., Brewer, W. A., ... & Angevine, W. M. (2006). Turbulent bulk transfer coefficients and ozone deposition velocity in the International Consortium for Atmospheric Research into Transport and Transformation. *Journal of Geophysical Research: Atmospheres*, *111*(D23).

Fang, F., Zhu, Y., Zhang, X., Chen, J., Yu, H., Wang, Q., & Niu, Y. (2025). Dynamic coupled Atmosphere-Ocean-Wave modeling for enhanced coastal wind resource assessment. *Renewable Energy*, 124240.

French, J. R., Drennan, W. M., Zhang, J. A., & Black, P. G. (2007). Turbulent fluxes in the hurricane boundary layer. Part I: Momentum flux. *Journal of the atmospheric sciences*, *64*(4), 1089-1102.

Fuchs, R., Musial, W., Zuckerman, G. R., Chetan, M., Marquis, M., Rese, L., Cooperman, A., Duffy, P., Green, R., Beiter, P., Mulas Hernando, D., Morris, J. A., Jr., Randall, A., Jossart, J. A., Mudd, L., & Vickery, P. (2023). *Assessment of offshore wind energy opportunities and challenges in the U.S. Gulf of Mexico* (NREL/TP-5000-88195). National Renewable Energy Laboratory. https://www.nrel.gov/docs/fy24osti/88195.pdf

Gadad, S., & Deka, P. C. (2016). Offshore wind power resource assessment using Oceansat-2 scatterometer data at a regional scale. *Applied Energy*, *176*, 157-170.

Grachev, A. A., Leo, L. S., Fernando, H. J., Fairall, C. W., Creegan, E., Blomquist, B. W., ... & Hocut, C. M. (2018). Air–sea/land interaction in the coastal zone. *Boundary-layer meteorology*, *167*(2), 181-210.

Golzio, A., Bollati, I. M., & Ferrarese, S. (2019). An assessment of coordinate rotation methods in sonic anemometer measurements of turbulent fluxes over complex mountainous terrain. *Atmosphere*, *10*(6), 324.

https://doi.org/10.5194/wes-2026-21
Preprint. Discussion started: 12 February 2026

He, Y., Fu, J., Chan, P. W., Li, Q., Shu, Z., & Zhou, K. (2021). Reduced sea-surface roughness length at a coastal site. *Atmosphere*, *12*(8), 991.

He, R., Wang, Q., Du, X., Luo, K., & Fan, J. (2025). Boundary layer dynamics and power performance of an offshore wind farm during unstable ocean-wave-atmosphere interactions. *Energy*, 137461.

Hesp, P. A., Smyth, T. A., Nielsen, P., Walker, I. J., Bauer, B. O., & Davidson-Arnott, R. (2015). Flow deflection over a foredune. *Geomorphology*, *230*, 64-74.

Högström, U. L. F. (1988). Non-dimensional wind and temperature profiles in the atmospheric surface layer: A re-evaluation. *Boundary-Layer Meteorology*, *42*(1), 55-78.

Holman, R. A., & Stanley, J. (2007). The history and technical capabilities of Argus. *Coastal engineering*, *54*(6-7), 477-491.

ICF. (2021). Comparison of environmental effects from different offshore wind turbine foundations (OCS Study BOEM 2021-053) (48 pp.). U.S. Department of the Interior, Bureau of Ocean Energy Management, Headquarters, Sterling, VA.

Izumi, Y. (1971). *Kansas 1968 field program data report* (No. 379). Air Force Cambridge Research Laboratories, Air Force Systems Command, United States Air Force.

Kitaigorodskii, S. A., & Donelan, M. A. (1984). Wind-wave effects on gas transfer. In Gas transfer at water surfaces (pp. 147-170). Dordrecht: Springer Netherlands.

Kljun, N., Calanca, P., Rotach, M. W., & Schmid, H. P. (2015). A simple two-dimensional parameterisation for Flux Footprint Prediction (FFP). *Geoscientific Model Development*, *8*(11), 3695-3713.

Landberg, L. (2015). *Meteorology for wind energy: an introduction*. John Wiley & Sons.

Lavers, D. A., Beljaars, A., Richardson, D. S., Rodwell, M. J., & Pappenberger, F. (2019). A forecast evaluation of planetary boundary layer height over the ocean. *Journal of Geophysical Research: Atmospheres*, *124*(9), 4975-4984.

Laskowicz, T. (2022). Offshore wind energy potential in Europe: a forecast of installed capacities and costs. *Europa Xxi*, *42*, 129-148.

Lentz, S. J., Davis, K. A., Churchill, J. H., & DeCarlo, T. M. (2017). Coral Reef Drag Coefficients – Water Depth Dependence. *Journal of Physical Oceanography*, *47*(5), 1061–1075.

Li, Z., Song, L., Ma, H., Xiao, J., Wang, K., & Chen, L. (2018). Observed surface wind speed declining induced by urbanization in East China. *Climate Dynamics*, *50*(3), 735-749.

Liu, W. T., Tang, W., & Xie, X. (2008). Wind power distribution over the ocean. *Geophysical research letters*, *35*(13).

Long, C. E., & Oltman-Shay, J. M. (1991). Directional characteristics of waves in shallow water. Coastal engineering research center Vicksburg MS.

Luu, L. N., van Meijgaard, E., Philip, S. Y., Kew, S. F., de Baar, J. H., & Stepek, A. (2023). Impact of surface roughness changes on surface wind speed over western Europe: A study with the regional climate model RACMO. *Journal of Geophysical Research: Atmospheres*, *128*(12), e2022JD038426.

Lyu, M., Potter, H., & Collins, C. O. (2021). The impacts of gustiness on Air–Sea momentum flux. *Fluids,* 6(10), 336.

https://doi.org/10.5194/wes-2026-21
Preprint. Discussion started: 12 February 2026

Mahrt, L., Vickers, D., Howell, J., Højstrup, J., Wilczak, J. M., Edson, J., & Hare, J. (1996). Sea surface drag coefficients in the Risø Air Sea Experiment. *Journal of Geophysical Research: Oceans*, *101*(C6), 14327-14335.

Mahrt, L., Miller, S., Hristov, T., & Edson, J. (2018). On estimating the surface wind stress over the sea. *Journal of Physical Oceanography*, *48*(7), 1533-1541.

585 Monin, A. S., & Obukhov, A. M. (1954). Basic laws of turbulent mixing in the surface layer of the atmosphere. *Contrib. Geophys. Inst. Acad. Sci. USSR*, *151*(163), e187.

National Renewable Energy Laboratory. (2025). Coastal Wind Resource Assessment Wind Research NREL. National Renewable Energy Laboratory. https://www.nrel.gov/wind/offshore-resource.

Obukhov, A. M. (1946). 'Turbulentnost' v temperaturnoj–neodnorodnoj atmosfere (Turbulence in an atmosphere with a non-uniform temperature). *Tr. Akad. Nauk. SSSR Inst. Teorel. Geofiz*., 1, 95–115.

Ortiz-Suslow, D. G., Haus, B. K., Williams, N. J., Laxague, N. J. M., Reniers, A. J. H. M., & Graber, H. C. (2015). The spatial-temporal variability of air-sea momentum fluxes observed at a tidal inlet. *Journal of Geophysical Research: Oceans*, *120*(2), 660-676.

Ortiz-Suslow, D. G., Kalogiros, J., Yamaguchi, R., & Wang, Q. (2021). An evaluation of the constant flux layer in the atmospheric flow above the wavy air-sea interface. *Journal of Geophysical Research: Atmospheres*, *126*(8), e2020JD032834.

Porchetta, S., Muñoz-Esparza, D., Munters, W., van Beeck, J., & van Lipzig, N. (2021). Impact of ocean waves on offshore wind farm power production. *Renewable Energy*, *180*, 1179-1193.

Potter, H. (2015). Swell and the drag coefficient. *Ocean Dynamics*, *65*(3), 375-384.

Potter, H., Collins III, C. O., Drennan, W. M., & Graber, H. C. (2015b). Observations of wind stress direction during Typhoon Chaba (2010). *Geophysical Research Letters*, *42*(22), 9898-9905.

Potter, H., Graber, H. C., Williams, N. J., Collins III, C. O., Ramos, R. J., & Drennan, W. M. (2015). In situ measurements of momentum fluxes in typhoons. *Journal of the Atmospheric Sciences*, *72*(1), 104-118.

Potter, H., Collins, C. O., & Ortiz-Suslow, D. G. (2022). Pier-based measurements of air-sea momentum fluxes over shoaling waves during DUNEX. *Journal of Geophysical Research: Oceans*, *127*(11), e2022JC018801.

605 Potter, H., Lyu, M., & Yang, X. (2025). Elevated Momentum Flux in the Surfzone during a Storm. *Journal of the Atmospheric Sciences*, *82*(7), 1237-1247.

Sathe, A., Mann, J., Barlas, T., Bierbooms, W. A., & van Bussel, G. J. (2013). Influence of atmospheric stability on wind turbine loads. *Wind energy*, *16*(7), 1013-1032.

Schumann, E. H., & Martin, J. A. (1991). Climatological aspects of the coastal wind field at Cape Town, Port Elizabeth and Durban. *South African Geographical Journal*, *73*(2), 48-51.

Schwarz, C., Van Starrenburg, C., Donker, J., & Ruessink, G. (2021). Wind and sand transport across a vegetated foredune slope. *Journal of Geophysical Research: Earth Surface*, *126*(1), e2020JF005732.

Shabani, B., Nielsen, P., & Baldock, T. (2014). Direct measurements of wind stress over the surf zone. *Journal of Geophysical Research: Oceans*, *119*(5), 2949-2973.

Shabani, B., Babanin, A. V., & Baldock, T. E. (2016). Observations of the directional distribution of the wind energy input function over swell waves. *Journal of Geophysical Research: Oceans*, *121*(2), 1174-1193.

Smedman, A. S., Bergström, H., & Högström, U. (1995). Spectra, variances and length scales in a marine stable boundary layer dominated by a low level jet. *Boundary-Layer Meteorology*, *76*(3), 211-232.

Smedman, A. S., Högström, U., & Bergström, H. (1997). The turbulence regime of a very stable marine airflow with quasi-frictional decoupling. *Journal of Geophysical Research: Oceans*, *102*(C9), 21049-21059.

Smith, S. D. (1980). Wind stress and heat flux over the ocean in gale force winds. *Journal of Physical Oceanography*, *10*(5), 709-726.

Smith, S. D., Anderson, R. J., Oost, W. A., Kraan, C., Maat, N., De Cosmo, J., ... & Chadwick, H. M. (1992). Sea surface wind stress and drag coefficients: The HEXOS results. *Boundary-layer meteorology*, *60*(1), 109-142.

Stull, R. B. (2012). *An introduction to boundary layer meteorology* (Vol. 13). Springer Science & Business Media.

Sullivan, P. P., Edson, J. B., Hristov, T., & McWilliams, J. C. (2008). Large-eddy simulations and observations of atmospheric marine boundary layers above nonequilibrium surface waves. *Journal of the Atmospheric Sciences*, *65*(4), 1225-1245.

Swinbank, W. C. (1964). The exponential wind profile. *Quarterly Journal of the Royal Meteorological Society*, *90*(384), 119-135.]

Swinbank, W. C., & Dyer, A. J. (1967). An experimental study in micro-meteorology. *Quarterly Journal of the Royal Meteorological Society*, *93*(398), 494-500.

U.S. Census Bureau. (2019). Coastline America [Infographic]. U.S. Census Bureau. https://www.census.gov/library/visualizations/2019/demo/coastline-america.html.

Wang, J., Feng, J., Yan, Z., & Zha, J. (2020). Urbanization impact on regional wind stilling: A modeling study in the Beijing-Tianjin-Hebei region of China. *Journal of Geophysical Research: Atmospheres*, *125*(20), e2020JD033132.

Webb, E. K. (1970). Profile relationships: The log-linear range, and extension to strong stability. *Quarterly Journal of the Royal Meteorological Society*, *96*(407), 67-90.

Wever, N. (2012). Quantifying trends in surface roughness and the effect on surface wind speed observations. Journal of Geophysical Research: Atmospheres, 117(D11).

WindEurope. (2021). Offshore wind in Europe: Key trends and statistics 2020. WindEurope. https://windeurope.org/data/products/offshore-wind-in-europe-2020/

Wiser, R., Lantz, E., Mai, T., Zayas, J., DeMeo, E., Eugeni, E., ... & Tusing, R. (2015). Wind vision: A new era for wind power in the United States. *The Electricity Journal*, *28*(9), 120-132.

Wu, L., Shao, M., & Sahlée, E. (2020). Impact of air–wave–sea coupling on the simulation of offshore wind and wave energy potentials. *Atmosphere*, *11*(4), 327.

Yang, B., Qian, Y., Berg, L. K., Ma, P. L., Wharton, S., Bulaevskaya, V., ... & Shaw, W. J. (2017). Sensitivity of turbine-height wind speeds to parameters in planetary boundary-layer and surface-layer schemes in the weather research and forecasting model. *Boundary-layer meteorology*, *162*(1), 117-142.

https://doi.org/10.5194/wes-2026-21
Preprint. Discussion started: 12 February 2026

Yang, Z., Calderer, A., He, S., Sotiropoulos, F., Doyle, J. D., Flagg, D. D., ... & Shen, L. (2018). Numerical study on the effect of air–sea–land interaction on the atmospheric boundary layer in coastal area. *Atmosphere*, *9*(2), 51.

Yuan, Q., Wang, S., Wang, B., Jing, R., & Chen, B. (2026). The influence of wave steepness and age on wake dynamics and power performance of offshore wind farms. *Applied Energy*, *404*, 127147.